# On the interplay between strain rate and strain rate sensitivity on flow localization in the dynamic expansion of ductile rings

G. Vadillo, J.A. Rodríguez-Martínez *, J. Fernández-Sáez

*Department of Continuum Mechanics and Structural Analysis, University Carlos III of Madrid, Avda. de la Universidad, 30, 28911 Leganés, Madrid, Spain*

*Keywords:*
Strain rate
Strain rate sensitivity
Flow localization
Stability analysis
Ring expansion

A B S T R A C T

In this work a stability analysis on flow localization in the dynamic expansion of ductile rings is con ducted. Within a 1 D theoretical framework, the boundary value problem of a radially expanding thin ring is posed. Based on a previous work, the equations governing the stretching process of the expanding ring are derived and solved using a linear perturbation method. Then, three different perfectly plastic material constitutive behaviours are analysed: the rate independent material, the rate dependent mate rial showing constant logarithmic rate sensitivity and the rate dependent material showing non constant and non monotonic logarithmic rate sensitivity. The latter allows to investigate the interaction between inertia and strain rate sensitivity on necking formation. The main feature of this work is rationally dem onstrate that under certain loading conditions and material behaviours: (1) decreasing rate sensitivity may not lead to more unstable material, (2) increasing loading rate may not lead to more stable material. This finding reveals that the relation between rate sensitivity and loading rate controls the unstable flow growth. Additionally a finite element model of the ring expansion problem is built in ABAQUS/Explicit. The stability analysis properly reflects the results obtained from the numerical simulations. Both proce dures, perturbation analysis and numerical simulations, allow for emphasizing the interplay between rate sensitivity and inertia on strain localization.

## 1. Introduction

The study of materials subjected to extreme loading conditions such as crash, impact, or explosion, has become increasingly rele vant in the modern industry. Today, engineering fields such as the aeronautical, automotive, and naval industries require accurate knowledge of the high rate failure of engineering materials. The study has taken in account accidental loads such as collisions, explosions, and penetration by fragments in the design of offshore structures (Borvik et al., 2003; Hopperstad et al., 2003). The ability for energy absorption has to be evaluated in the manufacturing of mechanical parts for vehicles, vessels, and aircraft (Borvik et al., 2003; Abramowicz and Jones, 1984a,b; Durrenberger et al., 2006). In addition, many of the physical phenomena involved in structural impact situations are also relevant in machining opera tions and forming processes.

It has been well established since the time of Considère (1885) that the development of plastic instabilities is closely related to ductile failure (Papirno et al., 1980; Couque, 1998; Molinari et al., 2002; Rodríguez Martínez et al., 2010). Understanding the forma tion and propagation of instabilities offers significant steps towards optimising the behaviour of materials at high strain rates. Susceptibility of materials to strain localization determines the suitability of their energy absorption under dynamic solicitations. A precise knowledge of the causes behind instabilities formation is required to construct mechanical elements meant to absorb energy under impact.

Within the framework of strain localization, a large body of lit erature has been devoted to studying dynamic necking. In the wake of the pioneering experimental works of Mann (1936) and Clark and Wood (1957) strain instability in tensile specimens sub jected to uniaxial impact has attracted the attention of researchers over recent decades (Klepaczko, 1968, 2005; Rusinek et al., 2005). The effect of impact velocity on failure energy has been examined, and enhanced ductility of the samples with an increasing loading rate has been detected for different materials within certain range of impact velocities. However, this loading configuration admits a maximum impact velocity, which leads to a sudden drop in mate rial ductility. This is the critical impact velocity (CIV). The CIV occurs when the speed of plastic waves approximates zero due to localization of plastic deformation (Kàrman and Duwez, 1950; Taylor, 1958) and imposes an upper limit to the dynamic tension test for determining material properties.

In an effort to avoid this drawback for evaluating material ductility at high deformation rates, the ring expansion test was

* Corresponding author. Tel.: +34 91 624 8460; fax: +34 91 624 9430.
*E-mail address:* jarmarti@ing.uc3m.es (J.A. Rodríguez-Martínez).

developed (Niordson, 1965). In this test a ring is subjected to uni form radial expansion. The material stretches during loading until homogeneous deformation fails at large strain, leading to flow local ization in the form of necking. Complications resulting from wave propagation are eliminated due to the symmetry of the problem (Hu and Daehn, 1996; Mercier and Molinari, 2004; Rusinek and Zae ra, 2007). This test is meant to evaluate the influence of deformation velocity on ductility, virtually without limits on velocity. Over the last few decades, experimental results for different metals and alloys have suggested that ductility is an increasing function of applied velocity (Grady and Brenson, 1983; Hu and Daehn, 1996; Altynova et al., 1996; Zhang and Ravi Chandar, 2006, 2008). For further understanding of this phenomenon a significant number of theoret ical models have been published (Hutchinson and Neale, 1977; Fres sengeas and Molinari, 1985; Sorensen and Freund, 2000; Guduru and Freund, 2002; Mercier and Molinari, 2004; Zhou et al., 2006; Shenoy and Freund, 1999). It has been established that high velocity ductility is controlled by inertia and material constitutive behaviour. The role played by forces of inertia in strain localization has been in tensely investigated (Grady, 1982; Rajendran and Fyfe, 1982; She noy and Freund, 1999). It has been determined that inertia diffuses deformation throughout the material, delaying plastic localization. The role played by the constitutive behaviour of the material may be split into the effect of strain hardening and the effect of rate sen sitivity (Ghosh, 1977; Altynova et al., 1996; Vela et al., 2011), both helping to stabilize material behaviour (Zhou et al., 2006; Xue et al., 2008).

These investigations have resulted in a rational explanation of the roles that, inertia, strain hardening, and strain rate sensitivity play individually on flow instability. However, as pointed out else where (Xue et al., 2008), the combined effect of inertia and mate rial constitutive behaviour on plastic localization still requires further research.

Thus, the present study analyses the interplay between inertia and material rate sensitivity on flow instability in the dynamic expansion of ductile rings. Based on the work of Zhou et al. (2006), a linear perturbation method is used to examine flow local ization for three different perfectly plastic material behaviours: the rate independent material, the rate dependent material showing constant logarithmic rate sensitivity and the rate dependent mate rial showing non constant and non monotonic logarithmic rate sensitivity. The latter reveals that, under certain loading condi tions, ductility may not be an increasing function of loading rate and/or rate sensitivity. It is rationally demonstrated that interac tion between inertia and material constitutive description is responsible for this behaviour. Finally, a finite element model of the ring expansion problem is built in ABAQUS/Explicit. The stabil ity analysis properly captures the results of the numerical simulations.

## 2. Problem formulation and stability analysis

In this section, following the procedure developed by Zhou et al. (2006), the boundary value problem of a radially expanding thin ring is formulated. Within a 1 D theoretical framework, the equa tions governing the stretching process of the expanding ring are derived and solved using a linear perturbation method.

### 2.1. Governing equations

Based on Zhou et al. (2006) the ring expansion process is approximated to a cylindrical bar with cross section radius $r_0$, area $A_0 \quad \pi r_0^2$, and length $L$ subjected to axial velocity $v_0$ and uniform tensile strain rate $\dot{\varepsilon}$. At time $t$ and for any cross section of the bar, $X$ is the Lagrangian coordinate $X(0 \leqslant X \leqslant L)$, $x$ is the Eulerian coordinate, $v$ the current axial velocity, $r$ and $A$ the current radius and cross sectional area, respectively, and $\sigma$ the true stress. The fundamental equations of the loading process are presented below:

$$\begin{cases} \left(\frac{\partial v}{\partial X}\right)_t \quad e^{\varepsilon}\dot{\varepsilon} \\ \rho_0 A_0 \left(\frac{\partial v}{\partial t}\right)_X \quad A\left(\frac{\partial \sigma}{\partial X}\right)_t + \sigma\left(\frac{\partial A}{\partial X}\right)_t \\ A \quad A_0 e^{\varepsilon} \\ \sigma_y \quad \Psi(\varepsilon, \dot{\varepsilon}) \\ \sigma \quad (1+\theta\ ^1) ln(1+\theta)\sigma_y \\ \theta \quad \frac{1}{2} r\left(\frac{\partial^2 r}{\partial x^2}\right) \quad \frac{2A\left(\partial^2 A/\partial x^2\right)\ (\partial A/\partial x)^2}{8\pi\sqrt{A}} \end{cases} \tag{1}$$

where $\varepsilon \quad ln\left[\left(\frac{\partial x}{\partial X}\right)_t\right]$ is the true strain, $\dot{\varepsilon} \quad (\partial\varepsilon/\partial t)$ is the strain rate, $\rho_0$ is the material density, $\sigma_y \quad \Psi(\varepsilon, \dot{\varepsilon})$ is the material yield stress and $\theta$ is a geometrical parameter which takes into account the effect of hydrostatic pressure on the notched section (Walsh, 1977; Bridg man, 1952).

Now let us set the initial and boundary conditions for a bar sub jected to constant and uniform strain rate

$$v(X,0) \quad \dot{\varepsilon}_0 X \quad v(0,t) \quad 0 \quad v(L,t) \quad \dot{\varepsilon}_0 L \tag{2}$$

According to Eq. (2), the system of equations given by Eq. (1) has the following homogeneous solution:

$$f_1 \quad (v_1(X), \varepsilon_1(t), \dot{\varepsilon}_1(t), A_1(t), r_1(t), \sigma_1(t), \theta_1)^T \tag{3}$$

This defines the background state of the boundary value problem in absence of flow instability. Further details can be found in Zhou et al. (2006).

### 2.2. Linear perturbation analysis

Following Zhou et al. (2006), a small perturbation of the type

$$\delta f e^{i\xi X} \quad (\delta v, \delta\varepsilon, \delta\dot{\varepsilon}, \delta A, \delta r, \delta\theta, \delta\sigma)^T e^{i\xi X} \tag{4}$$

is added to the background state solution defined by Eq. (3) at a gi ven time $t_0$. In previous expression $\xi$ is the wavenumber and $(\delta v, \delta\varepsilon, \delta\dot{\varepsilon}, \delta A, \delta r, \delta\theta, \delta\sigma)$ are the differences between the actual per turbed solution and the homogeneous solution.

Then, at a time $t > t_0$ the perturbed solution of the aforemen tioned system of equations has the following form:

$$f \quad f_1 + \delta f e^{i\xi X + \eta(t\ \ t_0)} \tag{5}$$

where $\eta$ is the perturbation growth rate which is assumed time independent.

Introducing Eq. (5) into Eq. (1) and keeping only the first order terms, the following linear homogeneous system is derived:

$$\begin{cases} i\xi\ ^1 e^{\varepsilon_1(t_0)}[\delta\dot{\varepsilon} + \dot{\varepsilon}_1(t_0)\delta\varepsilon] + \delta v \quad 0 \\ \eta\delta\varepsilon \quad \delta\dot{\varepsilon} \quad 0 \\ A_1(t_0)\delta\varepsilon + \delta A \quad 0 \\ \delta A/2\sqrt{\pi A_1(t_0)} \quad \delta r \quad 0 \\ \frac{\partial\Psi}{\partial\varepsilon}\delta\varepsilon + \frac{\partial\Psi}{\partial\dot{\varepsilon}}\delta\dot{\varepsilon} + \frac{1}{2}\sigma_1(t_0)\delta\theta \quad \delta\sigma \quad 0 \\ \frac{\xi^2}{4\pi} e^{\ 2\varepsilon_1(t_0)}\delta A + \delta\theta \quad 0 \\ i\xi[A_1(t_0)\delta\sigma + \sigma_1(t_0)\delta A] \quad \rho_0 A_0 \eta\delta v \quad 0 \end{cases} \tag{6}$$

An non trivial solution for $\delta f$ can be derived if the determinant of the previous system of algebraic linear equations is equal to zero. This leads to the following quadratic expression in $\eta$

$$\eta^2 + \left[\dot{\varepsilon}_1(t_0) + \frac{\xi^2}{\rho_0} e^{\ 2\varepsilon_1(t_0)} \frac{\partial\Psi}{\partial\dot{\varepsilon}}\right]\eta + \frac{\xi^2}{\rho_0} e^{\ 2\varepsilon_1(t_0)}\left[\frac{\partial\Psi}{\partial\varepsilon} + \sigma_1(t_0)\left(\frac{A_0 e^{\ 3\varepsilon_1(t_0)}}{8\pi}\xi^2 \quad 1\right)\right] \quad 0 \tag{7}$$

At this point, according to Zhou et al. (2006), the following dimen sionless variables are introduced:

$$\eta \quad \frac{\eta}{\dot{\varepsilon}_1} \quad \xi \quad r_0\xi \tag{8}$$

where $\bar{\eta}$ is the dimensionless perturbation growth and $\bar{\xi}$ is the dimensionless wavenumber.

Additionally, in this work, let us identify the following set of dimensionless variables:

$$\begin{aligned} &p \quad \varepsilon \quad \dot{p} \quad \frac{\dot{\varepsilon}}{\dot{\varepsilon}_0} \quad \Psi(\varepsilon,\dot{\varepsilon}) \quad \sigma_0\psi(p,\dot{p}) \\ &\bar{L} \quad K_L\frac{\sqrt{\psi(p_1,\dot{p}_1)}}{\dot{p}_1} \quad K_L \quad \frac{\sqrt{\sigma_0/\rho_0}}{r_0\dot{\varepsilon}_0} \\ &\chi_m \quad \left(\frac{\dot{p}_1}{\psi(p_1,\dot{p}_1)}\right)\cdot\frac{\partial\psi(p,\dot{p})}{\partial\dot{p}} \quad \chi_n \quad \left(\frac{1}{\psi(p_1,\dot{p}_1)}\right)\cdot\frac{\partial\psi(p,\dot{p})}{\partial p} \end{aligned} \tag{9}$$

where $p$ is the strain, $\dot{p}$ is the dimensionless strain rate dependent on a reference strain rate $\dot{\varepsilon}_0, \sigma_0$ is a reference yield stress, $\psi(p,\dot{p})$ is the dimensionless material yield stress, $\bar{L}$ is a dimensionless length which gathers the loading rate effect, $K_L$ is a dimensionless material parameter which gathers geometrical and material effects (similar to that proposed by Mercier and Molinari (2003)), $\chi_m$ is the logarithmic rate sensitivity and $\chi_n$ is the dimensionless strain hard ening parameter.

Then, at the initial state $\varepsilon_1 = 0$, Eq. (7) takes the following form

$$\eta^2 + (1+\chi_m\bar{L}^2\xi^2)\eta + \bar{L}^2\xi^2\left(\chi_n + \frac{\xi^2}{8} \quad 1\right) \quad 0 \tag{10}$$

From this point on only perfectly plastic materials are considered, and therefore $\chi_n = 0$. Thus, the condition for the perturbation growth is $\bar{\xi} < 2\sqrt{2}$. As reported elsewhere (Hill and Hutchinson, 1975; Shenoy and Freund, 1999; Mercier and Molinari, 2004) short er wavelength (larger wavenumber) perturbations are suppressed due to inertia. If the condition $\bar{\xi} < 2\sqrt{2}$ is fulfilled, the perturbation growth is defined by

$$\eta^+ \quad \frac{(1+\chi_m\bar{L}^2\xi^2) + \sqrt{(1+\chi_m\bar{L}^2\xi^2)^2 + 4\bar{L}^2\xi^2\left(1 \quad \frac{\xi^2}{8}\right)}}{2} \tag{11}$$

Imposing $\frac{\partial\eta^+}{\partial\xi}$ 0 in Eq. (11) the dominant wavenumber $\bar{\xi}_c$ and the critical perturbation growth $\bar{\eta}_c^+$ are determined as

$$\begin{aligned} &\xi_c \quad \left[\frac{2(2+\chi_m) \quad 2\chi_m\sqrt{1+8(1+\chi_m)\bar{L}^2}}{1 \quad 2\chi_m^2\bar{L}^2}\right]^{0.5} \\ &\eta_c^+ \quad \eta^+(\xi_c) \end{aligned} \tag{12}$$

For the study of the stabilizing effects of inertia and rate sensitivity for different constitutive descriptions, the sign of $\frac{d\eta_c^+}{dp}$ needs to be analysed. This task is approached in the following sections.

## 3. Stability analysis results for different material behaviours

In this section the influence of strain rate and strain rate sensi tivity on flow localization is examined. Based on the stability anal ysis presented above, three different material constitutive equations will be analysed:

1. Rate independent material.
2. Rate dependent material: The case of constant logarithmic rate sensitivity.
3. Rate dependent material: The case of non constant and non monotonic logarithmic rate sensitivity.

The reference material parameters used for the analysis are listed in Table 1.

### 3.1. Rate independent material

For a rate independent material, the yield stress is defined by the following equation:

$$\sigma_y \quad \Psi \quad \sigma_0 \tag{13}$$

For which $\chi_m = 0$ and therefore the critical wavenumber remains constant $\bar{\xi}_c$ 2 as discussed elsewhere (Zhou et al., 2006; Walsh, 1977). Then the critical perturbation growth $\bar{\eta}_c^+$ is given by

$$\eta_c^+ \quad \frac{1+\sqrt{1+8\bar{L}^2}}{2} \tag{14}$$

This is a decreasing power type concave up function of the dimen sionless strain rate $\dot{p}$ as illustrated in Fig. 1. The material stabilizes with increasing loading rate ($d\bar{\eta}_c^+/d\dot{p} < 0$) and decreasing $K_L$ (which gathers the influence of inertia via material density, Eq. (9)).

Forces of inertia are responsible for such behaviour (Hu and Daehn, 1996; Altynova et al., 1996; Rajendran and Fyfe, 1982; Xue et al., 2008). It is widely accepted that inertia enhances ductil ity by diffusing deformation throughout the material and retarding necking formation (Altynova et al., 1996; Xue et al., 2008). There fore, similar results (based on rate independent material configura tions) reported elsewhere over the years (Altynova et al., 1996) have suggested that improved ductility at high loading rates is due mainly to the role played by inertia. This point will be dis cussed in the following sections of this work.

### 3.2. Rate dependent material: The case of constant logarithmic strain rate sensitivity

For a rate dependent material defined by a power type rate hardening formulation, the yield stress is defined by the following equation:

$$\sigma_y \quad \Psi(\dot{\varepsilon}) \quad \sigma_0(\dot{\varepsilon}/\dot{\varepsilon}_0)^m \quad \sigma_0\psi(\dot{p}) \tag{15}$$

According to Eq. (9) this formulation defines the logarithmic strain rate sensitivity parameter as a constant $\chi_m = m = cte$. This material definition has been frequently considered in the literature (Mercier and Molinari, 2004; Zhou et al., 2006; Hu and Daehn, 1996; Xue et al., 2008) for analysing the effect of rate sensitivity on flow instability.

Next, let us depict the evolution of the dimensionless flow stress $\psi(\dot{p})$ as a function of the dimensionless rate parameter $\dot{p}$ for different values of the dimensionless rate sensitivity $\chi_m$, Fig. 2. The derivative $d\psi/d\dot{p}$ significantly increases with $\chi_m$. Thus, for low values of $\dot{p}$ the smaller dimensionless flow stress corre sponds to the larger value of the rate sensitivity parameter $\chi_m = 0.5$. Beyond certain value of $\dot{p}$ the opposite trend is observed.

The evolution of the dominant wavenumber $\bar{\xi}_c$ versus $\dot{p}$ is illus trated in Fig. 3a for several values of $\chi_m$. For all the cases consid ered, the critical wavenumber $\bar{\xi}_c$ increases with loading rate (Mercier and Molinari, 2004; Zhou et al., 2006; Guduru and Freund, 2002). The growth of the critical wavenumber is asymptotic to $\bar{\xi}_c$ 2. This is consistent with the observations reported elsewhere (Zhou et al., 2006). It should be noted that, as discussed by Mercier and Molinari (2004), an increase in $\chi_m$ reduces the value of $\bar{\xi}_c$. Rate

**Table 1**
Reference material parameters used in the analysis.

| $r_0(m)$ | $\sigma_0(Pa)$ | $\rho_0(\mathrm{kg/m^3})$ | $\varepsilon_0(s^{-1})$ |
|---|---|---|---|
| $5\times10^{-4}$ | $500\times10^6$ | 7800 | 10000 |

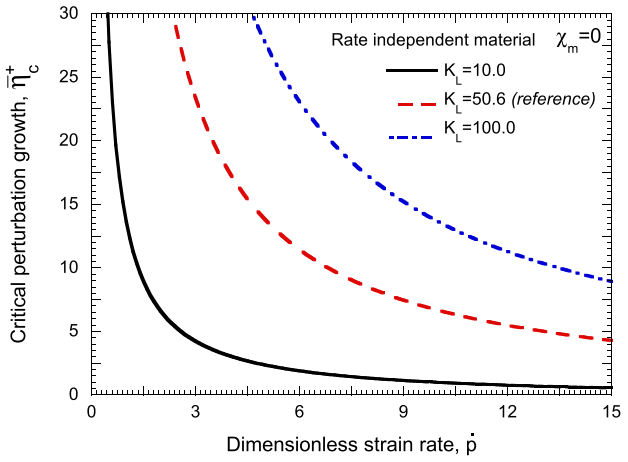


**Fig. 1.** Rate independent material. Critical perturbation growth $\eta_c^+$ as a function of dimensionless strain rate $p$ for several values of $K_L$.

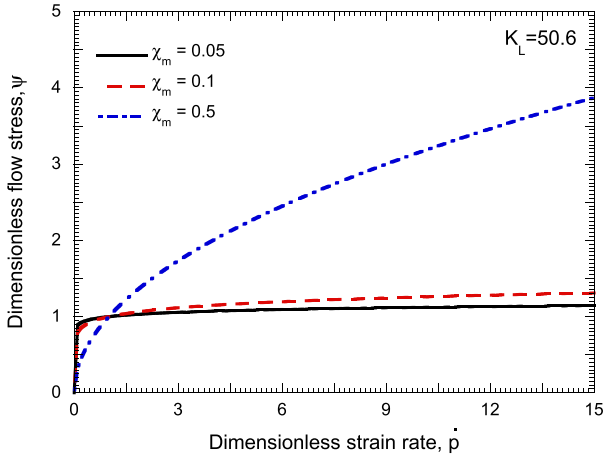


**Fig. 2.** Rate dependent material: the case of constant logarithmic strain rate sensitivity. Dimensionless flow stress $\psi$ as a function of dimensionless strain rate $p$ for different values of $\chi_m$.

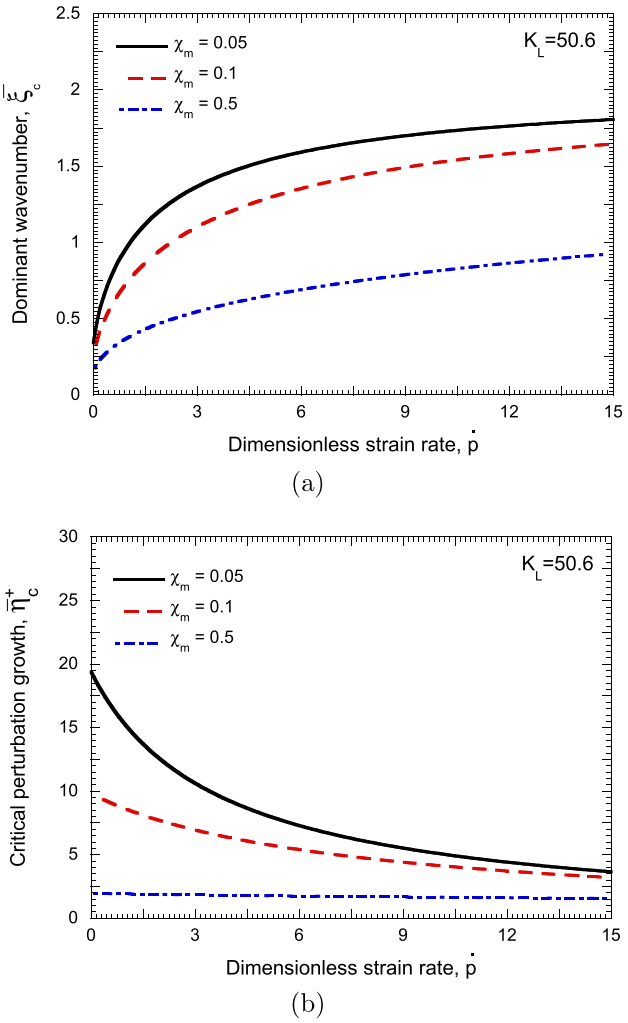


**Fig. 3.** Rate dependent material: the case of constant logarithmic strain rate sensitivity. (a) Dominant wavenumber $\xi_c$ as a function of dimensionless strain rate $p$ for different values of $\chi_m$. (b) Critical perturbation growth $\eta_c^+$ as a function of dimensionless strain rate $p$ for different values of $\chi_m$.

sensitivity promotes the growth of longer wavelength perturbations. The evolution of the critical perturbation growth $\bar{\eta}_c^+$ versus $\dot{p}$ is illustrated in Fig. 3b for several values of $\chi_m$. It decreases with the loading rate (due to inertia effects) $(d\bar{\eta}_c^+/d\dot{p} < 0)$ and with an increasing rate sensitivity parameter.

Thus, supported by experimental observations (Grady and Brenson, 1983; Ghosh, 1977; Zhang and Ravi Chandar, 2006, 2008) and theoretical models (Rajendran and Fyfe, 1982; Shenoy and Freund, 1999; Zhou et al., 2006) based on different rate independent and rate dependent materials, the following statements have been frequently accepted in the literature:

- Material stability increases with loading rate.
- Material stability increases with rate sensitivity.

However, these assumptions may not be fulfilled by rate dependent materials, showing non constant and non monotonic logarithmic rate sensitivity. It was already pointed out by Xue et al. (2008) that *"the interplay between material rate dependence and inertia in neck retardation is complex and dependent on the precise form of the constitutive model"*. In fact, under certain loading conditions, material stability may decrease with an increasing loading rate and/or logarithmic rate sensitivity, as it will be shown in the next section of this paper.

### *3.3. Rate dependent material: The case of non constant and non monotonic logarithmic strain rate sensitivity*

Considering a rate dependent material defined by an exponential type rate hardening formulation, the yield stress is determined by the following equation:

$$\sigma_y \quad \Psi(\dot{\varepsilon}) \quad \sigma_0(1 + k(1 \quad Exp(\ \dot{p}))) \quad \sigma_0\psi(\dot{p}) \tag{16}$$

where $k$ is a dimensionless parameter representative of the material rate sensitivity.

This formulation has been applied in constitutive modelling of metallic alloys which show athermal rate dependent straining within the high rate deformation regime (Nemat Nasser et al., 2001; Huang et al., 2009). This was concluded from the experimental evidence reported in the literature for a certain number of metals (Kapoor and Nemat Nasser, 1999; Nemat Nasser and Guo, 2000; Nemat Nasser et al., 2001). It attempts to provide a phenomenological description of the material structure evolution at high loading rates. According to Eq. (9), previous expression leads to a non constant and non monotonic logarithmic strain rate sensitivity parameter, $\chi_m$, as it is shown in Fig. 4b.

Next, the results from the stability analysis are presented. The purpose is to show the interplay between strain rate and strain rate

sensitivity on flow localization. For this task the analysis is split into two parts, first the effect of the dimensionless parameter $k$ is exam ined, and second the effect of the dimensionless parameter $K_L$.

*3.3.1. On the influence of the dimensionless parameter k*

The whole analysis conducted in this section has been carried out for $K_L = 50.6$ which results from the application of the reference material parameters listed in Table 1.

Fig. 4a illustrates the evolution of the dimensionless flow stress $\psi(\dot{p})$ versus the dimensionless strain rate parameter $\dot{p}$ for several values of $k$. It can be seen that, as the parameter $k$ increases, the function $\psi$ does also. Moreover, Fig. 4b depicts the evolution of the dimensionless rate sensitivity $\chi_m$ as a function of $\dot{p}$ for several values of $k$. The material rate sensitivity augments with increasing $k$. It has to be highlighted that a maximum of the dimensionless rate sensitivity appears ($\partial\chi_m/\partial\dot{p}$ 0). This maximum is reached for lower values of $\dot{p}$ with increasing $k$.

Thus, the first step is to illustrate the evolution of the dominant wavenumber $\bar{\xi}_c$ as a function of the dimensionless strain rate $\dot{p}$ for different values of $k$, Fig. 5a. In agreement with the results shown in previous section, the critical wavenumber augments with loading rate (inertia enhances the growth of shorter wavelengths (Mercier and Molinari, 2003, 2004; Mercier et al., 2010)) and diminishes with rate sensitivity (increasing rate sensitivity pro motes the growth of longer wavelengths (Mercier and Molinari, 2003, 2004)). In addition, the growth of the critical wavenumber remains asymptotic to $\bar{\xi}_c$ 2 for all the values of $k$ considered. But the difference between the results shown in Fig. 3a and those reported in Fig. 5a appears. It concerns the shape of the curve $\bar{\xi}_c$ $\dot{p}$. In Fig. 3a, the curve $\bar{\xi}_c$ $\dot{p}$ kept concave down within the whole analysis. However in Fig. 5a the curve $\bar{\xi}_c$ $\dot{p}$ turns from con cave up to concave down for certain value of $\dot{p}$ which is dependent on $k$. This illustrates the dependence of the dominant wavenumber $\bar{\xi}_c$ with the rate sensitivity $\chi_m$ shown in Eq. (12).

Moreover, Fig. 5b shows the dependence of the dimensionless critical perturbation growth $\bar{\eta}_c^+$ on the dimensionless rate parame ter $\dot{p}$ for different values of $k$. The lowest value of $k$ considered, $k = 0.01$ (which represents the lowest material rate sensitivity) leads to a continuous decrease of $\bar{\eta}_c^+$ with increasing $\dot{p}$. This is con sistent with the results shown in previous sections where the con dition $d\bar{\eta}_c^+/d\dot{p} < 0$ was fulfilled in any case considered. Because of the low material rate sensitivity in this case, $k = 0.01$, the perturba tion growth is basically controlled by inertia. However, as the value of $k$ augments, the evolution of $\bar{\eta}_c^+$ with $\dot{p}$ no longer continuously de creases with $\dot{p}$, but any of these conditions can be found $d\bar{\eta}_c^+/d\dot{p} \gtrless 0$ within certain ranges of $\dot{p}$. The material rate sensitivity becomes

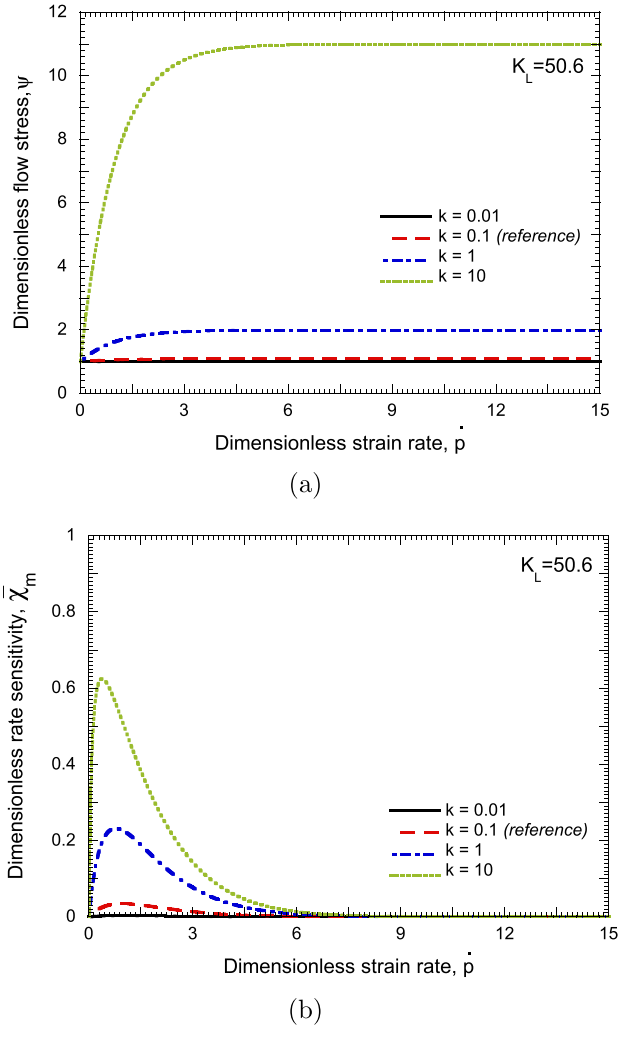


**Fig. 4.** Rate dependent material: the case of non-constant and non-monotonic logarithmic strain rate sensitivity. (a) Dimensionless flow stress $\psi$ as a function of dimensionless strain rate $p$ for different values of $k$. (b) Dimensionless rate sensitivity $\chi_m$ as a function of dimensionless strain rate $p$ for different values of $k$.

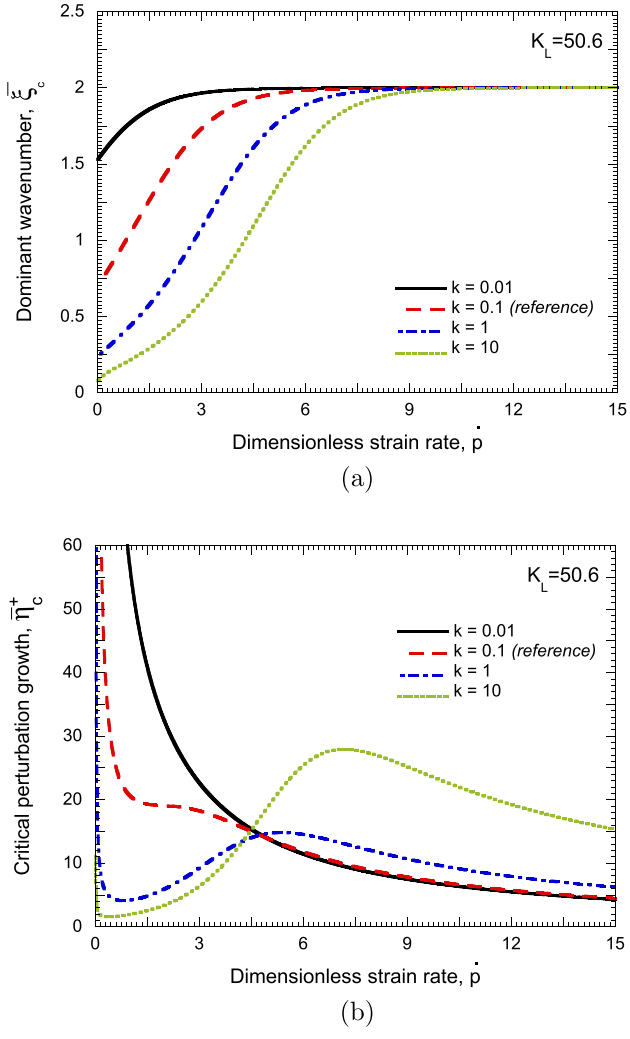


**Fig. 5.** Rate dependent material: the case of non-constant and non-monotonic logarithmic strain rate sensitivity. (a) Dominant wavenumber $\xi_c$ as a function of dimensionless strain rate $p$ for different values of $k$. (b) Critical perturbation growth $\eta_c^+$ as a function of dimensionless strain rate $p$ for different values of $k$.

influential on the perturbation growth. Thus, if $k = 0.1$ is considered, a point of inflection ($d\bar{\eta}_c^+/d\dot{p} \quad 0$ and $d^2\bar{\eta}_c^+/d\dot{p}^2 \quad 0$) is found for cer tain value of $\dot{p}$. Larger values of the parameter $k$ lead to the appear ance of relative minimum and maximum values in the $\bar{\eta}_c^+ \quad \dot{p}$ curve. Within the values of $\dot{p}$ corresponding to the local minimum and maximum the material does not stabilize with increasing loading rate. Note further that the relative minimum becomes smaller and the relative maximum becomes greater as $k$ increases. This finding has major relevance, since it demonstrates that, for certain loading conditions and material constitutive behaviours, an increasing strain rate does not bolster material stabilization and therefore an increasing strain rate does not augment ductility.

Fig. 6 illustrates the evolution of the dimensionless rate param eter $\dot{p}$ within the range $0.01 \leqslant k \leqslant 1000$, for which the following three conditions can be defined:

1. Maximum dimensionless rate sensitivity, $\chi_{m\ max}$.
2. Local minimum critical perturbation growth, $\bar{\eta}_{c\ min}^+$.
3. Local maximum critical perturbation growth, $\bar{\eta}_{c\ max}^+$.

According to this graph and following the idea reported in Xue et al. (2008) it is possible to establish a classification of the stability analysis results attending to the value of $k$.

- Region I $k \lesssim 0.1$: The curve $\bar{\eta}_c^+ \quad \dot{p}$ does not show relative maximum and minimum values. Perturbation growth continu ously diminishes with increasing loading rate. Material stability analysis is basically controlled by inertia. Decreasing rate sensi tivity does not lead to more unstable material.
- Region II $0.1 < k < 1$: The curve $\bar{\eta}_c^+ \quad \dot{p}$ shows relative maxi mum and minimum values. Material stability analysis is affected by inertia and strain rate sensitivity. Decreasing rate sensitivity may not lead to more unstable material. Increasing loading rate may not lead to more stable material.
- Region III $k \gtrsim 1$: The curve $\bar{\eta}_c^+ \quad \dot{p}$ shows relative maximum and minimum values. The relative minimum (most stabilized material) takes place at the value of $\dot{p}$ where the logarithmic rate sensitivity is maximum $\chi_{m\ max}$. Material stability analysis is basically controlled by rate sensitivity. Increasing loading rate may not lead to more stable material.

Up to this point it seems to be clear that, not only strain rate, but also strain rate sensitivity may play a major role on flow instability. However, further understanding on the interplay be tween strain rate and strain rate sensitivity on flow localization is required. For that task, let us depict the derivative of the critical perturbation growth with respect to the dimensionless rate param eter $d\bar{\eta}_c^+/d\dot{p}$ versus $\dot{p}$, Fig. 7.

This comes from the following analytical expression in which the terms related to the dimensionless strain rate sensitivity parameter $\chi_m$ can be adequately identified.

$$\frac{d\eta_c^+(\chi_m, \bar{L})}{d\dot{p}} \quad \frac{\partial \eta_c^+}{\partial \bar{L}} \frac{\partial \bar{L}}{\partial \dot{p}} + \frac{\partial \eta_c^+}{\partial \chi_m} \frac{\partial \chi_m}{\partial \dot{p}} \tag{17}$$

In the case of considering a rate independent material and/or a rate dependent material showing constant logarithmic rate sensitivity the terms related to the dimensionless strain rate sensitivity param eter $\chi_m$ are set to zero, $\frac{\partial \eta_c^+}{\partial \chi_m} \quad 0$ and $\frac{\partial \chi_m}{\partial \dot{p}} \quad 0$. Therefore, the appear ance of local minimum and maximum values in the curve $\bar{\eta}_c^+ \quad \dot{p}$ is expected to be related to any of these two terms. Let us check this hypothesis by means of the analysis conducted below.

Fig. 8 depicts those terms that are not related to the dimension less rate sensitivity parameter $\frac{\partial \eta_c^+}{\partial \bar{L}}$ and $\frac{\partial \bar{L}}{\partial \dot{p}}$, as a function of the dimensionless rate parameter $\dot{p}$ for different values of $k$.

- The term $\frac{\partial \eta_c^+}{\partial \bar{L}}$ increases with $\dot{p}$ following a sigmoidal shape and decreases with increasing value of $k$. It should be noted that this term remains positive regardless of the value of $k$.
- The term $\frac{\partial \bar{L}}{\partial \dot{p}}$ shows an exponential concave down shape which decreases with increasing $k$. It should be noted that it remains negative regardless of the value of $k$.

The product of previous factors $\frac{\partial \eta_c^+}{\partial \bar{L}} \frac{\partial \bar{L}}{\partial \dot{p}}$ remains negative for the entire range of $\dot{p}$ considered, Fig. 9. This multiplicative term stabi lizes material behaviour for any loading rate level. It is not respon sible for the relative minimum and maximum values displayed in Fig. 5b.

Fig. 10 depicts the terms that are related to the dimensionless rate sensitivity parameter, $\frac{\partial \eta_c^+}{\partial \chi_m}$ and $\frac{\partial \chi_m}{\partial \dot{p}}$, as a function of the dimen sionless rate parameter $\dot{p}$ for different values of $k$.

- The term $\frac{\partial \eta_c^+}{\partial \chi_m}$ is asymptotic to zero with increasing rate param eter $\dot{p}$. It should be noted that this term remains negative regardless of the value of $k$.
- The term $\frac{\partial \chi_m}{\partial \dot{p}}$ is asymptotic to zero too, but this term changes from positive to negative at low values of the dimensionless rate parameter $\dot{p}$.

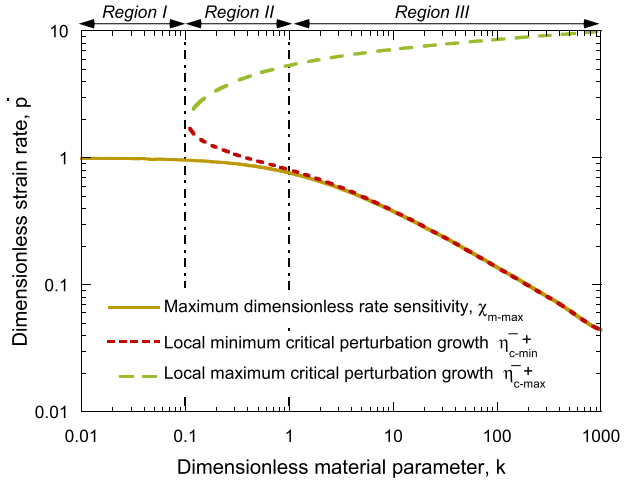


**Fig. 6.** Rate dependent material: the case of non-constant and non-monotonic logarithmic strain rate sensitivity. Dimensionless strain rate parameter $p$ as a function of the dimensionless material parameter $k$ for three different conditions. (1) Maximum dimensionless rate sensitivity, $\chi_{m\ max}$. (2) Local minimum critical perturbation growth, $\eta_{c\ min}^+$. (3) Local maximum critical perturbation growth, $\eta_{c\ max}^+$.

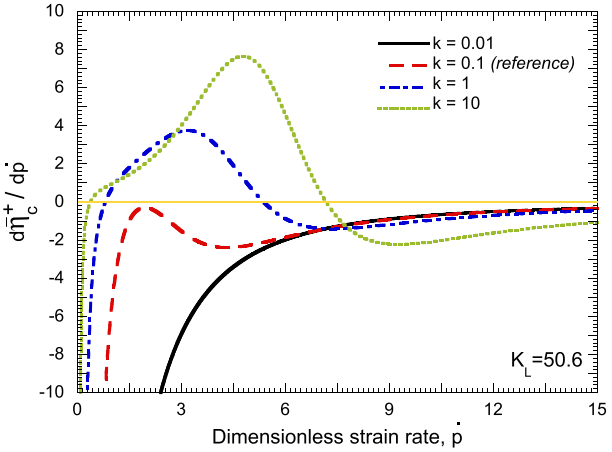


**Fig. 7.** Rate dependent material: the case of non-constant and non-monotonic logarithmic strain rate sensitivity. Derivative of the critical perturbation growth respect to the dimensionless loading rate $d\eta_c^+/dp$ versus $p$ for different values of $k$.

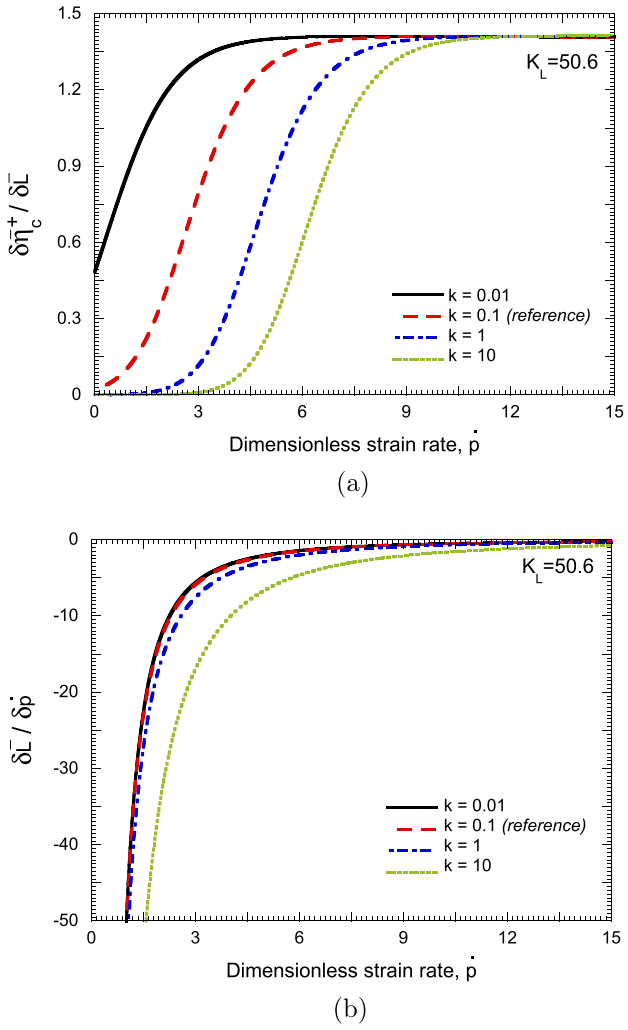


**Fig. 8.** Rate dependent material: the case of non-constant and non-monotonic logarithmic strain rate sensitivity. (a) Partial derivative of the critical perturbation growth respect to the dimensionless loading parameter $\frac{\partial \eta_c^+}{\partial \bar{L}}$ versus $p$ for different values of $k$. (b) Partial derivative of the dimensionless loading parameter respect to the dimensionless strain rate $\frac{\partial \bar{L}}{\partial \dot{p}}$ versus $p$ for different values of $k$.

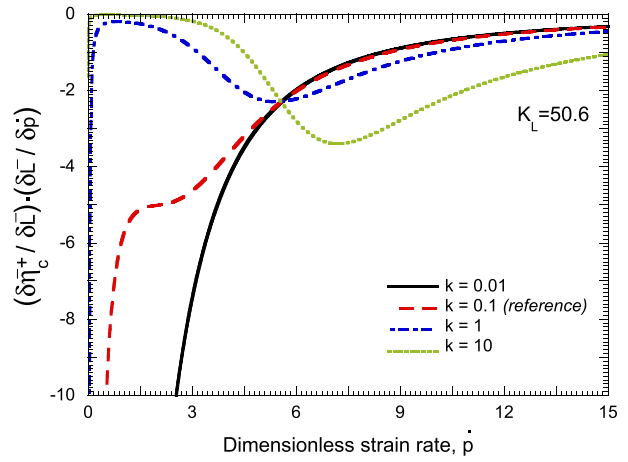


**Fig. 9.** Rate dependent material: the case of non-constant and non monotonic logarithmic strain rate sensitivity. The case of non-constant and non-monotonic logarithmic strain rate sensitivity. Evolution of $\frac{\partial \eta_c^+}{\partial \bar{L}} \frac{\partial \bar{L}}{\partial \dot{p}}$ versus $p$ for different values of $k$.

The product of previous factors $\frac{\partial \eta_c^+}{\partial \chi_m} \frac{\partial \chi_m}{\partial \dot{p}}$ remains negative for low values $\dot{p}$, Fig. 11. Then it changes to positive at a certain value of $\dot{p}$ which depends on $k$. Subsequently, it develops a local maximum and then it runs asymptotically to zero. This is responsible for the relative minimum and maximum values in Fig. 5b. Under cer tain loading conditions and material constitutive formulations this multiplicative term may not stabilize material behaviour with an increasing loading rate.

This finding reveals that the relation $\chi_m \quad \dot{p}$ determines the role played by rate sensitivity on unstable flow growth. Depending on the material rate sensitivity, it is possible that, under certain load ing conditions, decreasing rate sensitivity may not lead to more unstable material and/or that an increasing loading rate may not lead to more stable material.

### *3.3.2. On the influence of the dimensionless parameter $K_L$*

From this point on, let us conduct an analysis on the influence of $K_L$ (which gathers the effect of inertia via material density, Eq. (9); the parameter $K_L$ diminishes with increasing material density) on material stability. The dimensionless material parameter $k$ remains constant at a reference value $k = 0.1$. It should be noted that varia tions of $K_L$ do not affect the dimensionless flow stress $\psi(\dot{p})$.

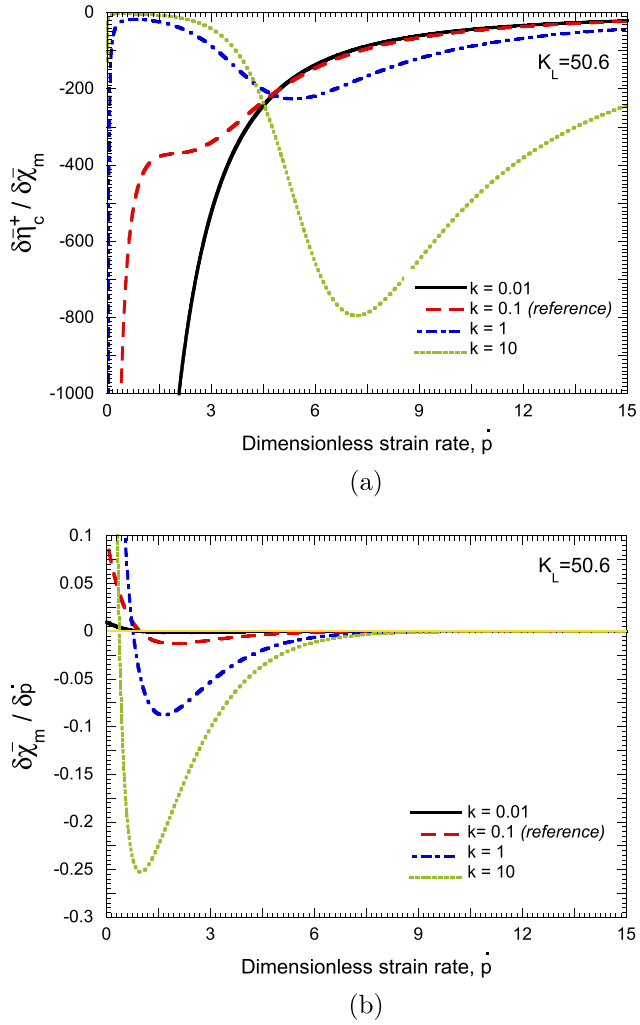


**Fig. 10.** Rate dependent material: the case of non-constant and non-monotonic logarithmic strain rate sensitivity. (a) Partial derivative of the critical perturbation growth respect to the dimensionless rate sensitivity $\frac{\partial \eta_c^+}{\partial \chi_m}$ versus $p$ for different values of $k$. (b) Partial derivative of the dimensionless rate sensitivity respect to the dimensionless strain rate $\frac{\partial \chi_m}{\partial \dot{p}}$ versus $p$ for different values of $k$.

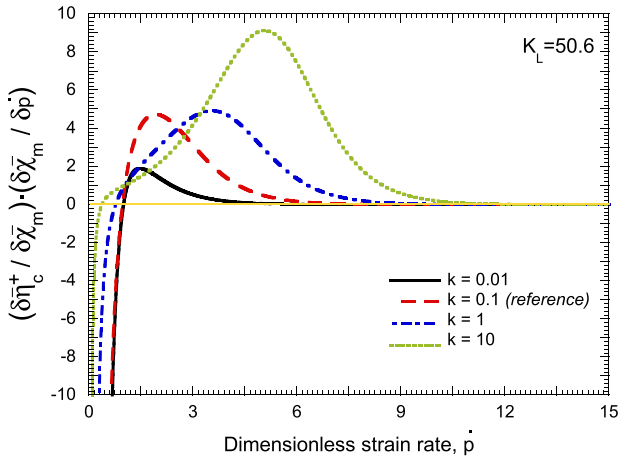


**Fig. 11.** Rate dependent material: the case of non-constant and non-monotonic logarithmic strain rate sensitivity. Evolution of $\frac{\partial \eta_c^+}{\partial \chi_m}\frac{\partial \chi_m}{\partial \dot{p}}$ versus $p$ for different values of $k$.

Fig. 12a depicts the change in the dominant wavenumber $\bar{\xi}_c$ as a function of the dimensionless strain rate $\dot{p}$ for different values of $K_L$. Decreasing values of $K_L$ boost the growth of short wavelength per turbations (Mercier and Molinari, 2003, 2004). Moreover, Fig. 12b illustrates the dependence of the dimensionless critical perturba tion growth $\bar{\eta}_c^+$ on the dimensionless rate parameter $\dot{p}$ for different values of $K_L$. It should be noted that for the lowest value of $K_L$ con sidered ($K_L = 10$) the material continuously stabilizes with an increasing loading rate, $d\bar{\eta}_c^+/d\dot{p} < 0$. When $K_L = 50.6$ (the reference case already discussed in Fig. 5b) a point of inflection takes place. Larger values of the parameter $K_L$ lead to a local minimum and maximum in the curve $\bar{\eta}_c^+$ $\dot{p}$. In other words, when low values of $K_L$ are taken into account, the growth of the perturbation is con trolled mainly by inertia, whereas when large values of $K_L$ are ta ken into account, the growth of the perturbation is controlled mainly by rate sensitivity, as was expected.

Again, a better understanding of this behaviour is achieved by analysing the derivative of the critical perturbation growth respect to the dimensionless rate parameter $d\bar{\eta}_c^+/d\dot{p}$ versus $\dot{p}$, Fig. 13.

This is split into two additive terms Eq. (17), as reflected in Fig. 14. The first term $\frac{\partial \eta_c^+}{\partial \bar{L}}\frac{\partial \bar{L}}{\partial \dot{p}}$ remains negative and runs asymptoti cally to zero. The second term $\frac{\partial \eta_c^+}{\partial \chi_m}\frac{\partial \chi_m}{\partial \dot{p}}$ remains negative for low val ues of $\dot{p}$ and subsequently becomes positive at certain values of $\dot{p}$ (quite regardless of $K_L$) and then it runs asymptotically to zero. The parameter $K_L$ controls the magnitude and amplitude of the po sitive part of the curve $\frac{\partial \eta_c^+}{\partial \chi_m}\frac{\partial \chi_m}{\partial \dot{p}}$ $\dot{p}$ and therefore determines the influence of rate sensitivity on the perturbation growth.

Next, finite element simulations of the rapid expansion of duc tile rings are conducted. The comparison is made between the sta bility analysis results and the numerical simulations.

## 4. Finite element simulation of the rapid expansion of ductile rings

A 3D finite element model of the rapid expansion of ductile rings is built in ABAQUS (2003) FE commercial code. The geometry and dimensions of the ring are based on the parameters listed in Table 1. The inner radius of the ring is $R_i = 15$ mm. The loading con dition is a radial velocity applied in the inner surface of the ring, which remains constant throughout the entire process (Rusinek and Zaera, 2007). These boundary conditions applied to the simu lations guarantee the uniaxial tensile state in the specimen during loading. The mesh used shows radial symmetry, no geometrical or material imperfections were introduced into the model (Larson et al., 1981) since they could perturb the necking process (Han and Tvergaard, 1995; Sorensen and Freund, 2000). The round off

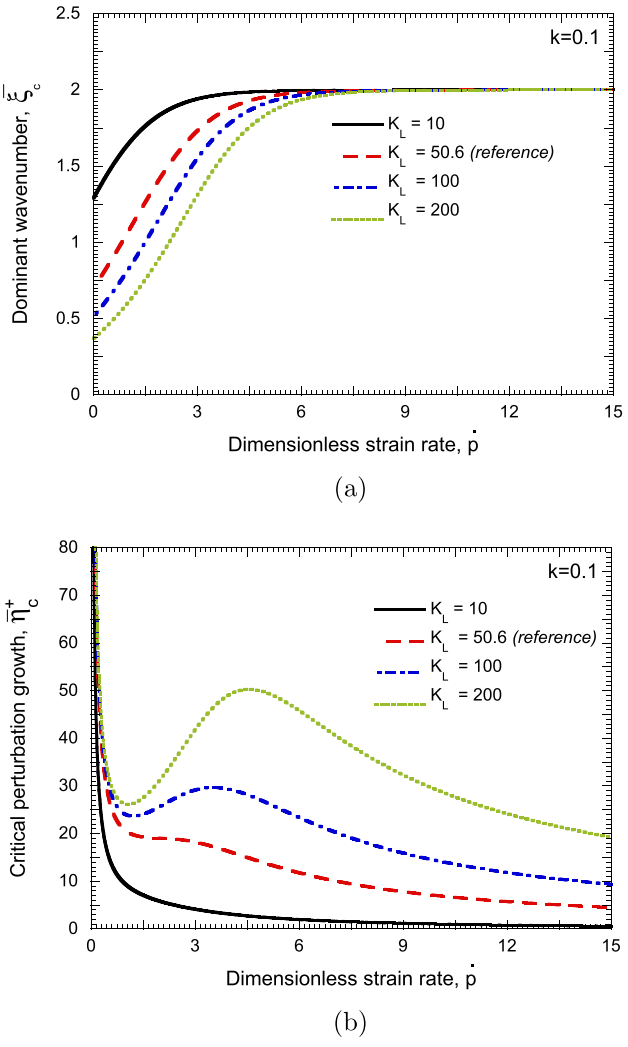


**Fig. 12.** Rate dependent material: the case of non-constant and non-monotonic logarithmic strain rate sensitivity. (a) Dominant wavenumber $\xi_c$ as a function of dimensionless strain rate $p$ for different values of $K_L$. (b) Critical perturbation growth $\eta_c^+$ as a function of dimensionless strain rate $p$ for different values of $K_L$.

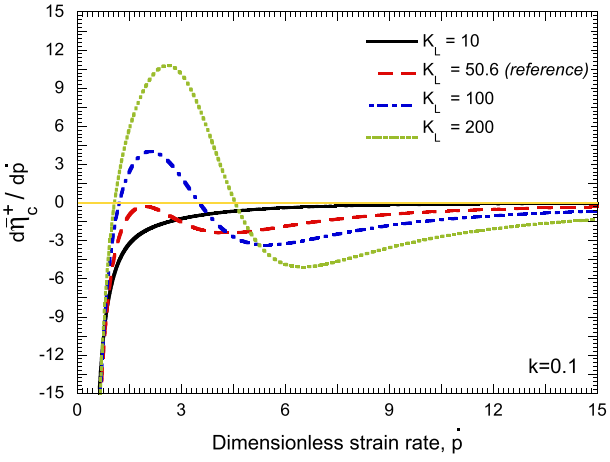


**Fig. 13.** Rate dependent material: the case of non-constant and non-monotonic logarithmic strain rate sensitivity. Derivative of the critical perturbation growth respect to the dimensionless loading rate $d\eta_c^+/dp$ versus $p$ for different values of $K_L$.

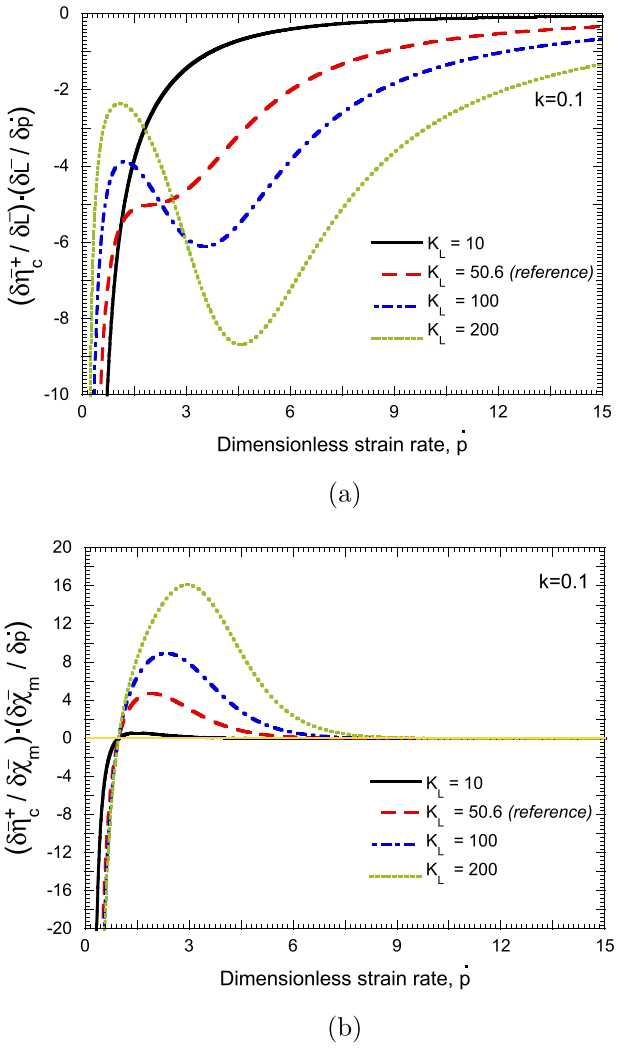


**Fig. 14.** Rate dependent material: the case of non-constant and non-monotonic logarithmic strain rate sensitivity. (a) Evolution of $\frac{\partial \eta_c^+}{\partial \bar{L}} \frac{\partial \bar{L}}{\partial \dot{p}}$ versus $p$ for different values of $K_L$. (b) Evolution of $\frac{\partial \eta_c^+}{\partial \chi_m} \frac{\partial \chi_m}{\partial \dot{p}}$ versus $p$ for different values of $K_L$.

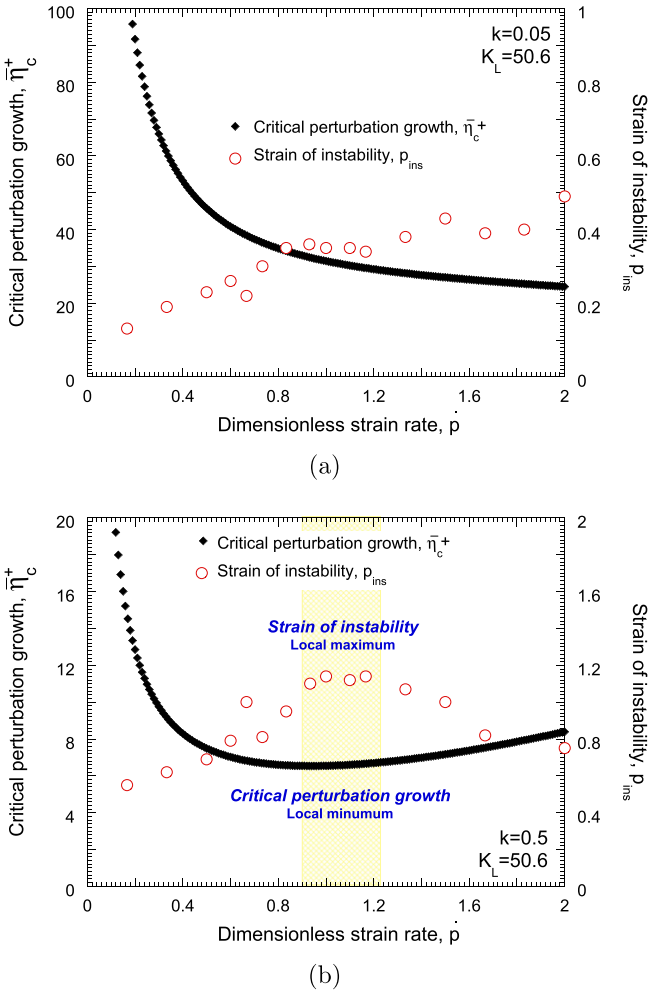


**Fig. 15.** Critical perturbation growth $\eta_c^+$ and strain of instability $p_{ins}$ obtained from the simulations as a function of dimensionless strain rate for $K_L = 50.6$. (a) $k = 0.05$ and (b) $k = 0.5$.

error through the integration process is enough to perturb the stress and strain fields (Rusinek and Zaera, 2007). Then, wave reflections and interactions take place, leading to flow localization in the absence of geometrical or material irregularities (Nemes and Eftis, 1993).

The material is modelled using the rate hardening law defined by Eq. (16). This has been implemented into ABAQUS/Explicit FE code via a user subroutine using the integration scheme for Hu ber Mises plasticity proposed by Zaera and Fernández Sáez (2006). Moreover, it should be noted that visco plasticity acts as a natural regularization method for solving mesh dependent strain softening problems of plasticity (Glema et al., 2000; Voyiadjis and Abed, 2006). This adequately helps to well pose the boundary va lue problem (Nemes and Eftis, 1993). Thus, the strain of instability (and therefore the number of necks formed) is a direct conse quence of the constitutive equations applied to describe the mate rial behaviour.

Numerical simulations are carried out within the range of dimensionless strain rate $0.1 \leqslant \dot{p} \leqslant 5$. The goal is to attain further validation of the results provided by the stability analysis. For this task, the strain of instability $p_{ins}$ (notice that $\varepsilon = p$) derived from the simulations is related to the critical perturbation growth $\bar{\eta}_c^+$ de rived from the stability analysis.

The strain of instability $p_{ins}$ is determined following the proce dure developed elsewhere (Rodríguez Martínez, 2010). Until neck ing takes place, the local plastic strain $p_{local}$ (plastic strain at a material point where necking will be formed) agrees with the glo bal plastic strain $p_{global}$ (theoretical deformation corresponding to homogeneous behaviour). Once the material flow becomes unsta ble, the local plastic strain drastically deviates from the global specimen deformation. According to Triantafyllidis and Waldenm yer (2004) the bifurcation point defines the strain of instability.

In Fig. 15, the critical perturbation growth $\bar{\eta}_c^+$ and the strain of instability $p_{ins}$ are depicted as a function of the dimensionless rate parameter $\dot{p}$ for two different values of $k$ while $K_L = 50.6$ remains constant.

The case of $k = 0.05$, Fig. 15a, fits within the region I shown in Fig. 6. The critical perturbation growth $\bar{\eta}_c^+$ continuously diminishes with loading rate $\dot{p}$, the process is controlled by inertia. Decreasing rate sensitivity does not lead to a more unstable material. This is properly reflected by the stability analysis, the strain of instability is an increasing function of the loading rate. This is considered rep resentative of a regular case analysed elsewhere (i.e. enhanced ductility with loading rate) (Rusinek and Zaera, 2007).

The case of $k = 0.5$, Fig. 15b, fits within the region II shown in Fig. 6. The critical perturbation growth $\bar{\eta}_c^+$ shows a local minimum (corresponding to local maximum of material stabilization) within the range of $\dot{p}$ considered. The process is influenced by rate sensitiv ity and inertia. Within a certain range of $\dot{p}$, the decreasing rate

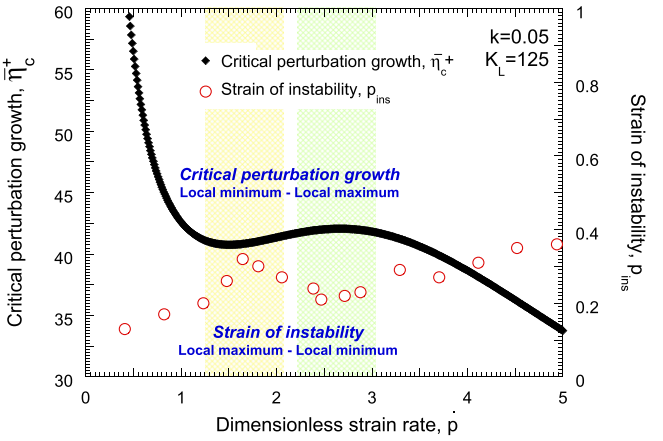


**Fig. 16.** Critical perturbation growth $\eta_c^+$ and strain of instability $p_{ins}$ as a function of dimensionless strain rate for $K_L = 125$ and $k = 0.05$.

sensitivity leads to more unstable material, but the maximum rate sensitivity does not coincide with the maximum material stabiliza tion. Again, the stability analysis properly reflects the material response predicted by the numerical simulations. The aforemen tioned local minimum of the perturbation growth agrees with the local maximum of the strain of instability.

Further validation of the stability analysis is shown in Fig. 16, where the critical perturbation growth $\bar{\eta}_c^+$ and the strain of insta bility $p_{ins}$ are depicted as a function of the dimensionless rate parameter $\dot{p}$ for $K_L = 125$ and $k = 0.05$. In this case, the critical per turbation growth $\bar{\eta}_c^+$ shows local minimum and maximum values within the range of $\dot{p}$ considered. Again, this behaviour is satisfac torily defined by the numerical simulations. Local minimum of the critical perturbation growth agrees with local maximum of the strain of instability and vice versa.

The results from the numerical simulations agree satisfactorily with the predictions made in the stability analysis. Both proce dures emphasize the interplay between rate sensitivity and inertia in flow instability.

## 5. Conclusions

Strain localization in ductile materials subjected to dynamic loading is a complex problem strongly influenced by material behaviour and inertia effects. In this work the effect of strain rate and strain rate sensitivity on flow instability in the dynamic expan sion of thin rings has been investigated using linear perturbation analysis. In this analysis, the essential dimensionless material parameters controlling the localization process have been ade quately identified. Relying on a perfectly plastic rate dependent material showing non constant and non monotonic logarithmic rate sensitivity, there are two main findings of the study:

- Under certain loading conditions decreasing rate sensitivity may not lead to a more unstable material.
- Under certain loading conditions increasing loading rate may not lead to a more stable material.

This behaviour comes from the interplay between inertia and material rate sensitivity on the strain localization process. The rela tion between rate sensitivity $\chi_m$ and loading rate $\dot{p}$ determines the role played by rate sensitivity on flow localization. Deformation re gimes in which inertia and/or rate sensitivity play the dominant role on necking formation have been identified. Additionally, a fi nite element model of the ring expansion problem was built in ABAQUS/Explicit. The stability analysis satisfactorily reflected the results of the numerical simulations.

## Acknowledgements

The authors express sincere gratitude to Prof. A. Rusinek for helpful discussions on the effect of material rate sensitivity on the formation of plastic instabilities in ductile materials.

The financial support of the Comunidad Autónoma de Madrid (Project CCG10 UC3M/DPI 5596) and of the Ministerio de Ciencia e Innovación de España (Project DPI/2008 06408) is kindly acknowledged.

## References

ABAQUS, 2003. Abaqus Explicit v6.4 User's Manual, version 6.4 Edition. ABAQUS Inc., Richmond, USA.
Abramowicz, W., Jones, N., 1984a. Dynamic axial crushing of circular tubes. International Journal of Impact Engineering 2, 263–281.
Abramowicz, W., Jones, N., 1984b. Dynamic axial crushing of square tubes. International Journal of Impact Engineering 2, 179–208.
Altynova, M., Hu, X., Daehn, G.S., 1996. Increased ductility in high velocity electromagnetic ring expansion. Metallurgical Transactions A 27, 1837–1844.
Borvik, T., Hopperstad, O.S., Berstad, T., 2003. On the influence of stress triaxiality and strain rate on the behaviour of a structural steel. Part II. Numerical study. European Journal of Mechanics A/Solids 22, 15–32.
Bridgman, P.W. 1952. Plastic wave in a wire extended by an impact load, Scientific papers, Mechanics of solids, New York: McGraw-Hill Book Company, Inc, vol. 1, pp. 9–37.
Clark, D.S., Wood, D.S., 1957. The influence of specimen dimension and shape on the results in tension impact testing. Transactions of the American Society of Mechanical Engineering, 577–585.
Considère, A.G., 1885. L'emploi du fer de l'acier dans les constructions. Annals Ponts et ChaussTes 9, 574–575.
Couque, H. 1998. On the use of the symmetric taylor test to evaluate dynamic ductile compression fracture properties of metals. In: 5th International Conference on Structures Under Shock and Impact, Computational Mechanics Inc, Billerica, MA, USA, pp. 579–589.
Durrenberger, L., Even, D., Molinari, A., Rusinek, A., 2006. Influence of the strain path on crash properties of a crash-box structure by experimental and numerical approaches. Journal of Physique IV 134, 1287–1293.
Fressengeas, C., Molinari, A., 1985. Inertia and thermal effects on the localization of plastic flow. Acta Metallurgica 33, 387–396.
Ghosh, A.K., 1977. Tensile instability and necking in materials with strain hardening and strain-rate hardening. Acta Metallurgica 25, 1413–1424.
Glema, A., Lodygowski, T., Perzyna, P., 2000. Interaction of deformation waves and localization phenomena in inelastic solids. Computers Methods in Applied Mechanics and Engineering 183, 123–140.
Grady, D.E., 1982. Local inertia effects in dynamic fragmentation. Journal of Applied Physics 1, 322–325.
Grady, D.E., Brenson, D.A., 1983. Fragmentation of metal rings by electromagnetic loading. Experimental Mechanics 12, 393–400.
Guduru, P.R., Freund, L.B., 2002. The dynamics of multiple neck formation and fragmentation in high rate extension of ductile materials. International Journal of Solids and Structures 39, 5615–5632.
Han, J.B., Tvergaard, V., 1995. Effect of inertia on the necking behaviour of ring specimens under rapid axial expansion. European Journal of Mechanics A/Solids 14, 287–307.
Hill, R., Hutchinson, J.W., 1975. Bifurcation phenomena in the plane tension test. Journal of the Mechanics and Physics of Solids 23, 239–264.
Hopperstad, O.S., Borvik, T., Langseth, M., Labibes, K., Albertini, C., 2003. On the influence of stress triaxiality and strain rate on the behaviour of a structural steel. Part I. Experiments. European Journal of Mechanics A/Solids 22, 1–13.
Hu, X., Daehn, G.S., 1996. Effect of velocity on flow localization in tension. Acta Materialia 44, 1021–1033.
Huang, M., del Castillo, P.E.J.R.-D., Bouaziz, O., der Zwaag, S.V., 2009. Deformation in fcc metals based on irreversible thermodynamics. Mechanics of Materials 41, 982–988.
Hutchinson, J.W., Neale, K.W., 1977. Influence of strain rate sensitivity on necking under uniaxial tension. Acta Metallurgica 25, 839–846.
Kapoor, R., Nemat-Nasser, S., 1999. Comparison between high strain-rate and low strain-rate deformation of tantalum. Metallurgical Materials Transactions A 31, 815–823.
Kàrman, T.V., Duwez, P., 1950. The propagation of plastic deformation in solids. Journal of Applied Physics 21, 987.
Klepaczko, J.R., 1968. Generalized conditions for instability in tension. International Journal of Mechanical Sciences 10, 297–313.
Klepaczko, J.R., 2005. Review on critical impact velocities in tension and shear. International Journal of Impact Engineering 32, 188–209.

Larson, M., Needlemen, A., Tvergaard, V., Storakers, B. 1981. Instability and failure of internally pressurized ductile metal cylinders. Technical report, Division of Engineering, Brown University.
Mann, H.C., 1936. High-velocity tension-impact tests. Proceedings ASTM 36, 85.
Mercier, S., Molinari, A., 2003. Predictions of bifurcations and instabilities during dynamic extensions. International Journal of Solids and Structures 40, 1995–2016.
Mercier, S., Molinari, A., 2004. Analysis of multiple necking in rings under rapid radial expansion. International Journal of Impact Engineering 4, 403–419.
Mercier, S., Granier, N., Molinari, A., Llorca, F., Buy, F., 2010. Multiple necking during the dynamic expansion of hemispherical metallic shells, from experiments to modelling. Journal of the Mechanics and Physics of Solids 58, 955–982.
Molinari, A., Musquar, C., Sutter, G., 2002. Adiabatic shear banding in high speed machining of Ti-6Al-4V: Experiments and modeling. International Journal of Plasticity 18, 443–459.
Nemat-Nasser, S., Guo, W., 2000. High strain-rate response of commercially pure vanadium. Mechanics of Materials 32, 243–260.
Nemat-Nasser, S., Guo, W.G., Khil, D.P., 2001. Thermomechanical response of AL-6XN stainless steel over a wide range of strain rates and temperatures. Journal of the Mechanics and Physics of Solids 49, 1823–1846.
Nemes, J.A., Eftis, J., 1993. Constitutive modelling on the dynamic fracture of smooth tensile bars. International Journal of Plasticity 9, 243–270.
Niordson, F.L., 1965. A unit for testing materials at high strain rates. Experimental Mechanics 5, 2932.
Papirno, R.P., Mescall, J.F., Hansen, A.M. 1980. Beyond the taylor test to fracture in designing for extremes: Environment, loading, and structural behavior. In: Proceedings of the Army Symposium on Solid Mechanics, Army Materials and Mechanics Research Center, pp. 579–589.
Rajendran, A.M., Fyfe, I.M., 1982. Inertia effects on the ductile failure of thin rings. Journal of Applied Mechanics 49, 31–36.
Rodríguez-Martínez, J.A. 2010. Advanced constitutive relations for modeling thermo-viscoplastic behaviour of metallic alloys subjected to impact loading. Ph.D. thesis, University Carlos III of Madrid-University, Paul Verlaine of Metz/ENIM.
Rodríguez-Martínez, J.A., Rusinek, A., Chevrier, P., Bernier, R., Arias, A., 2010. Temperature measurements on ES steel sheets subjected to perforation by hemispherical projectiles. International Journal of Impact Engineering 37, 828–841.
Rusinek, A., Zaera, R., 2007. Finite element simulation of steel ring fragmentation under radial expansion. International Journal of Impact Engineering 34, 799–822.
Rusinek, A., Zaera, R., Klepaczko, J.R., Cheriguene, R., 2005. Analysis of inertia and scale effects on dynamic neck formation during tension of sheet steel. Acta Materialia 53, 5387–5400.
Shenoy, V.B., Freund, L.B., 1999. Necking bifurcations during high strain rate extension. Journal of the Mechanics and Physics of Solids 47, 2209–2233.
Sorensen, N.J., Freund, L.B., 2000. Unstable neck formation in a ductile ring subjected to impulsive radial loading. International Journal of Solids and Structures 37, 2265–2283.
Taylor, G.I., 1958. Studies in Large Plastic Flow and Fracture, with Special Emphasis on the Effects of Hydrostatic Pressure. Cambridge University Press.
Triantafyllidis, N., Waldenmyer, J.R., 2004. Onset of necking in electro-magnetically formed rings. Journal of Mechanical Physics and Solids 52, 2127–2148.
Vela, C., Rodríguez-Martínez, J.A., Rusinek, A., 2011. FE analysis on the formation of plastic instabilities in dynamically expanded copper rings. Engineering Transactions 59, 1–23.
Voyiadjis, G.Z., Abed, F.H., 2006. A coupled temperature and strain rate dependent yield function for dynamic deformations of bcc metals. International Journal of Plasticity 22, 1398–1431.
Walsh, J.M., 1977. Plastic instability and particulation in stretching metals jets. Journal of Applied Physics 48, 4187–4195.
Xue, Z., Vaziri, A., Hutchinson, J.W., 2008. Material aspects of dynamic neck retardation. Journal of the Mechanics and Physics of Solids 56, 93–113.
Zaera, R., Fernández-Sáez, J., 2006. An implicit consistent algorithm for the integration of thermoviscoplastic constitutive equations in adiabatic conditions and finite deformations. International Journal of Solids and Structures 43, 1594–1612.
Zhang, H., Ravi-Chandar, K., 2006. On the dynamics of necking and fragmentation- I. Real-time and post-mortem observations in Al 6061-O. International Journal of Fracture 142, 183–217.
Zhang, H., Ravi-Chandar, K., 2008. On the dynamics of necking and fragmentation - II. Effect of material properties geometrical constraints and absolute size. International Journal of Fracture 150, 3–36.
Zhou, F., Molinari, J.F., Ramesh, K.T., 2006. An elasto-visco-plastic analysis of ductile expanding ring. International Journal of Impact Engineering 33, 880–891.